# Study on High-Cycle Fatigue Behaviors and Fracture Mechanism of RuT450

M. X. Zhang[a], J. C. Pang [a*, L.J.] Meng[a], S. X. Li[a], Q. Y. Liu[b],

A. L. Jiang[b] and Z. F. Zhang[a*]

[a]Shi-changxu Innovation Center for Advanced Materials, Institute of Metal Research, Chinese Academy of Sciences, 72 Wenhua Road, Shenyang 110016, PR China

[b] Weichai Power Co., Ltd., Weifang 261061, PR China

## Abstract:

Fatigue failure is the most common failure mode of structural materials. In this study, the high-cycle fatigue properties at different temperatures, fracture surface morphologies and corresponding damage mechanisms of a widely used vermicular graphite cast iron RuT450 were investigated. It is found that the fatigue strength of RuT450 decreases with the increase of temperature, and the decreasing rate is affected by the change of morphology and content of graphite. In general, the cracks initiated from the graphite phase boundary and propagated through the pearlite lamellae. In addition, according to the change of matrix micro-structure and the slight change of graphite morphology at different temperatures, and combined with the change of crack propagation threshold value under different temperature conditions, a fatigue strength prediction method for vermicular graphite cast iron at different temperatures was proposed in this work, which has high prediction accuracy.

***Key words*:** Vermicular graphite cast iron, Microstructures, High-cycle fatigue,

** Corresponding author

*E-mail: jcpang@imr.ac.cn (Jian Chao Pang); zhfzhang@imr.ac.cn (Zhe Feng Zhang).

Fracture mechanism, Fatigue strength prediction.

## 1. Introduction

With the rapid development of industry, diesel engine will occupy the mainstream position in the market at present and for a long time in the future [1]. Meanwhile, good thermal stability, excellent mechanical properties, excellent casting properties and low production cost make vermicular graphite cast iron playing an irreplaceable role in the field of diesel engine and other key components [2-4]. However, higher service temperature and frequent start-up and stop greatly limit the service time of cast iron components. According to the data statistics of failure analysis, the failure mode of most structural parts is fatigue fracture [5-6]. Therefore, the high cycle-fatigue (HCF) properties of vermicular graphite cast iron, especially in high temperature environment, should be paid more attentions. Above, reasonable fatigue fracture mechanism research and life prediction have important theoretical and engineering significance for the optimization of mechanical properties and reliability improvement of component materials [7-8].

At present, researchers have carried out some works on the fatigue properties of cast irons, mainly focusing on the fatigue behavior, damage mechanism and performance optimization [9-11]. Among them, the HCF behaviors of ductile cast iron have been widely concerned [12-14]. However, there are a few researches on vermicular graphite cast iron which is also widely used. Xu et al. [15] considered that the tensile strength and HCF limit of vermicular graphite cast iron decrease with the increase of vermicular rate, and graphite cluster is the main factor affecting the fatigue life, but its mechanism and strength prediction method are not pointed out. Liu et al. [16] demonstrated that the fatigue strength index and fatigue strength coefficient are linearly related to temperature, and this can be used to predict the fatigue life of cast iron. The HCF properties of vermicular graphite cast iron with different chemical composition and pearlite content have been systematically studied [17].

In addition, graphite morphology also plays an important role in fatigue strength. Although in recent years, people have carried out in-depth research on graphite morphology, such as Tartera et al. [18] proposed the growth theory and cluster distribution growth model of vermicular graphite. Chuang et al. [19] observed the spatial distribution of graphite in vermicular graphite cast iron. Liu et al. [20] characterized the three dimensional structure of graphite by X-ray; however, the effect of morphology on mechanical properties of cast iron is rarely studied.

In this study, one kind of vermicular graphite cast iron (RuT450) was employed for tensile and HCF tests at different temperatures. By means of metallographic structure and fracture analysis, the microstructure evolution of RuT450 at different temperatures was observed, and its fatigue fracture mechanism was analyzed too. According to the changing trend of microstructure transformation and graphite morphology, a formula suitable for predicting the fatigue strength of vermicular graphite cast iron at different temperatures was established.

## 2. Experimental materials and procedures

In this study, all samples were cut from the flame deck of the cylinder head. As shown in figure 1, HCF specimens with a total length of 90 mm and a gauge section of$\varphi$5 mm×17.5 mm were machined by using finish turning and followed by grinding. To avoid the negative effect of surface roughness, all specimens were polished with emery papers (#400, #800, #1200 and 2000# in order) along the axial direction.

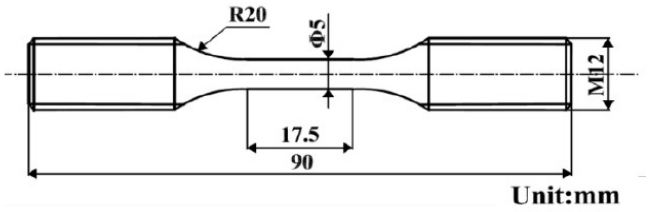


**Figure 1. Dimensions of fatigue test specimen.**

Stress-controlled symmetric push-pull fatigue was performed with a frequency of

about 110 Hz. An electromagnetic resonance fatigue testing machine Rumul Testronic 100 were employed to finish the fatigue tests under room temperature (RT), 400°C and 500°C in air. Sixteen to eighteen specimens were prepared for each temperature conditions. The run-out life is $10^7$ cycles. Staircase method (not less than five pairs of data) was employed to calculate the fatigue strength [21]. Tensile tests were conducted at a strain rate of $5\times10^{-4}s^{-1}$ by hydraulic servo testing machine Instron 5982 and micro-hardnesses were measured by an AMH43 automatic micro hardness tester. And the holding time of all high temperature samples is 30 min. All the fractographies, crack morphology and microstructure of RuT450 were observed by Quanta 600 scanning electron microscope (SEM). The chemical composition of RuT450 is shown in Table 1.

**Table 1. The chemical composition (*wt*%) of RuT450**

| Material | C | Si | Mn | S | P | Cu |
|---|---|---|---|---|---|---|
| RuT450 | 3.60 | 2.05 | 0.19 | 0.011 | 0.015 | 0.82 |

## 3. Experimental results

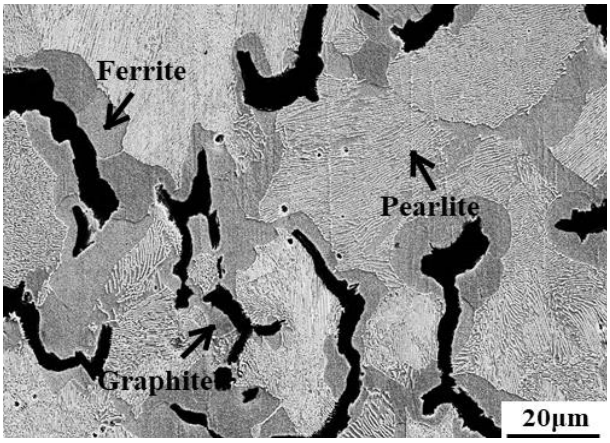


**Figure 2. The microstructure of RuT450.**

As shown in Fig. 2, the microstructure of RuT450 consists of three parts: the white zone is laminar pearlite which accounts for 80%, the gray zone is equiaxed

ferrite which accounts for 15%, and the rest black zone is graphite, both the percentages are area ones. The vermicular rate (the area rate of vermicular graphite to the all graphite) was 84%.

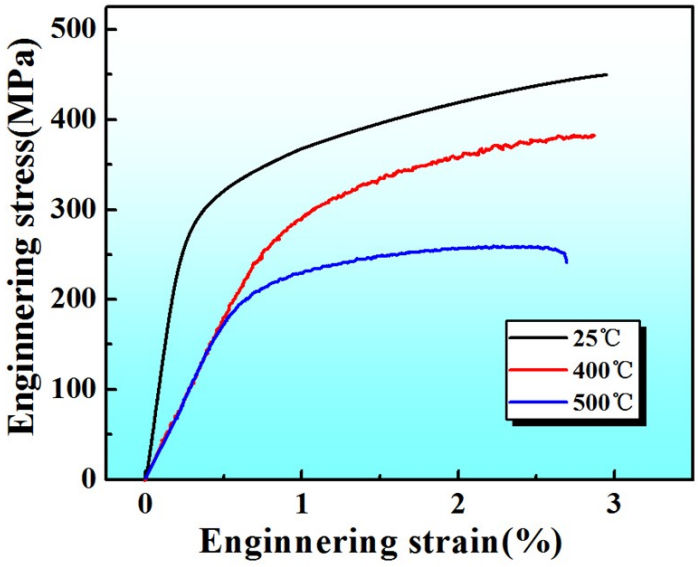


**Figure 3. Tensile engineering stress-strain curves of RuT450 at different temperatures.**

Tensile engineering stress-strain curves of RuT450 at different temperatures are shown in Fig. 3. Serrated fluctuation can be observed in the work-hardening stage of the stress-strain curves at 400°C and 500°C. Both the strength and elongation decrease at high temperature, it means that dynamic strain aging occurs [22-23].

The *S-N* curves of HCF are shown in Fig. 4 in which the red arrows indicate that the specimens do not fail up to $10^7$ cycles under the specific stress amplitude. The fatigue strength values are 150 MPa, 143 MPa and 108 MPa for RT, 400°C and 500°C, respectively. Compared with Figs. 4a, b and c, it can be seen that the dispersion of fatigue data under 400°C is narrower than that of other conditions. The slope (absolute value) of the curves increases with the increase of temperature, but the slopes are very close under 400°C and 500°C (Fig. 4d). The corresponding Basquin formulas are as follows:

$$\sigma_a = \sigma_f'(2N_f)^b = 319.41(2N_f)^{-0.047}, \quad \text{for RT (1)}$$

$$\sigma_a = \sigma_f'(2N_f)^b = 322.58(2N_f)^{-0.054}, \quad \text{for 400°C (2)}$$

$$\sigma_a = \sigma_f'(2N_f)^b = 267.46(2N_f)^{-0.056}, \quad \text{for 500°C (3)}$$

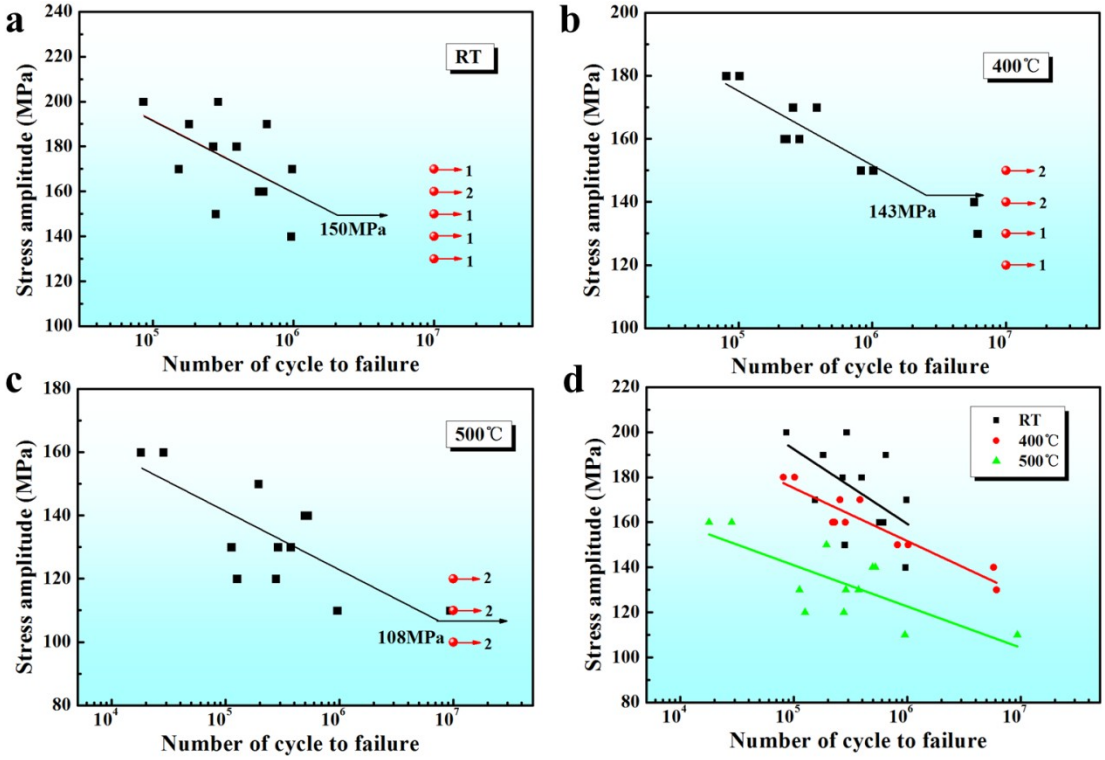


**Figure 4. The *S-N* curves and fatigue strengths at three different temperatures**

**(a)RT; (b)400℃; (c)500℃ and (d) the comparison of three curves.**

Samples with the same stress amplitude (160MPa) were selected for each temperature (the fatigue life at RT, 400°C and 500°C are 6112275, 219493 and 17889 cycles respectively), and the fatigue fractographies were observed by SEM, as shown in Fig. 5. It can be seen that both the fatigue source and the propagation zone are relatively flat in the fracture surface. Moreover, the areas of fatigue source and low speed propagation zone (inside the black dotted line in Figs. 5a, c and e) are much

smaller than that of the high-speed propagation and transient breaking area. With the increase of temperature, the proportion of propagation area decreases gradually, the value of RT is 7.7%, 400°C is 5.7% and 500°C is only 2.9%. In Fig.s 5b, d and f, it can be found that the fatigue sources are mainly concentrated on the surface of the specimen. Therefore, it can be preliminarily inferred that the crack initiation mechanism of vermicular graphite cast iron is the same under different temperatures under HCF conditions, but the propagation process is different.

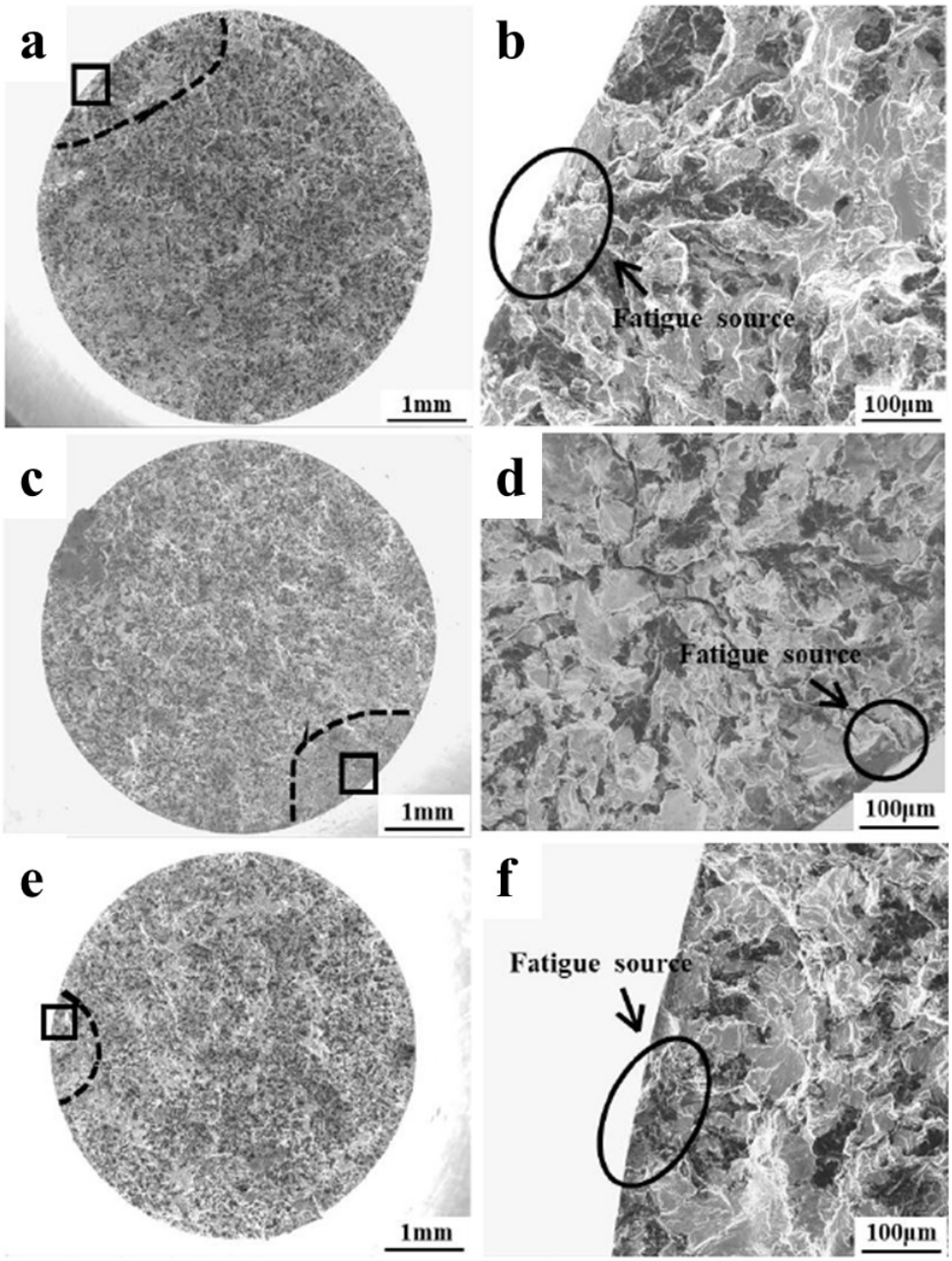


**Figure 5. Fatigue fracture morphologies at different temperatures:**

**(a) (b) RT, $N_f$=6112275; (c) (d) 400℃, $N_f$=219493; (e) (f) 500℃, $N_f$=17889.**

In order to further observe the crack propagation characteristics, the side metallographic observation of the above fracture samples is carried out, as shown in Fig. 6, Fig. 7 and Fig. 8. Figs. 6a, 7a and 8a show the growth path of fatigue main crack at different temperatures. It can be seen that the initiation and early propagation of fatigue crack are slow, and the fracture surface is relatively smooth. However, with the growth of the main crack, the crack propagation speed is accelerated. And the crack surface becomes rough, which reflected in the transverse fracture surface is the uneven crack profile in the instantaneous fracture zone.

It can be observed that the secondary crack initiation is caused by the debonding between vermicular graphite and matrix. At the same time, the secondary cracks appear at the graphite tip and propagate to the matrix. The propagation path of secondary crack can be divided into two types. One is that the secondary crack initiated from the graphite tip, then propagated to ferrite, then expanded in pearlite until it contacted another graphite tip (Figs. 6c, 7b and 8b). The other is that the secondary crack propagated directly to pearlite region without ferrite after initiation from graphite tip (Figs. 6d, 7d and 8c). The propagation direction of secondary crack can be mainly attributed into two groups. One is parallel to the main crack propagation direction (Figs. 6b, 7d and 8b). The other is nearly perpendicular to the main crack growth direction (Fig. 6c, 7c and 8c). Oxide layer at the edge of secondary crack can be found at high temperature (Figs. 8c and Fig. 8d).

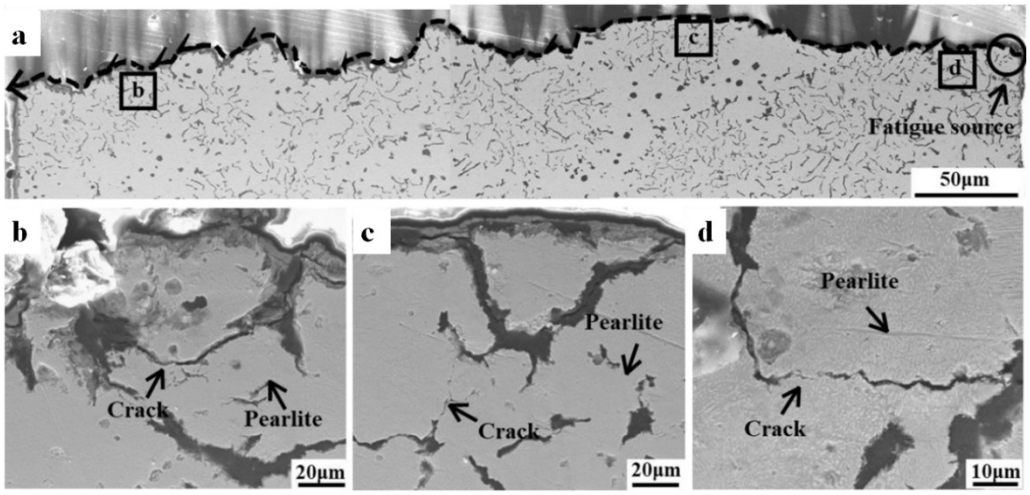


**Figure 6. Longitudinal section of the fatigue fractured specimen under RT ($\sigma_a$ =160MPa, $N_f$ =6112275).**

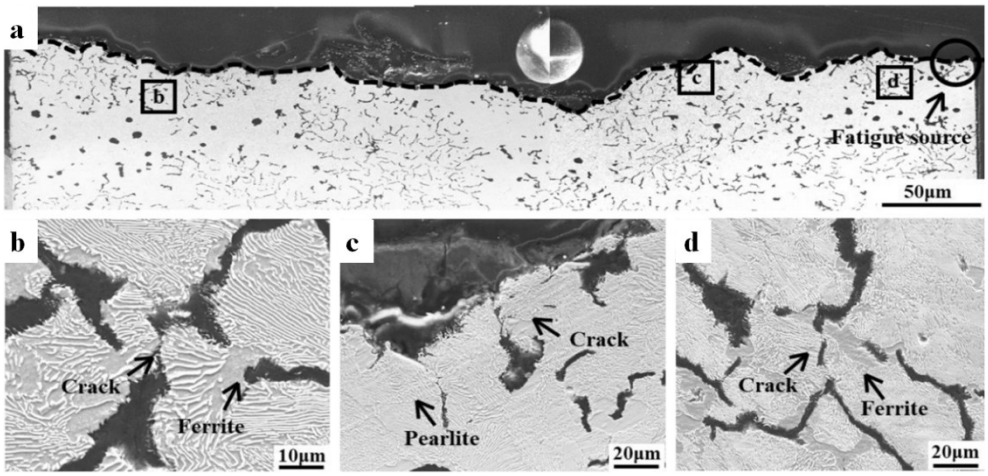


**Figure 7. Longitudinal section of the fatigue fractured specimen under 400℃ ($\sigma_a$ =160MPa, $N_f$ =219493).**

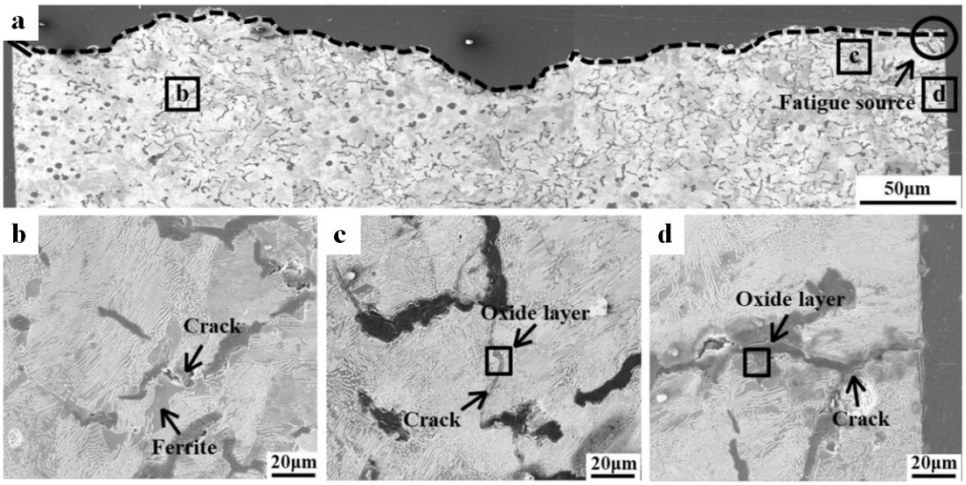


**Figure 8. Longitudinal section of the fatigue fractured specimen under 500℃ ($\sigma_a$ =160MPa, $N_f$ =17889).**

According to the previous research results, the tensile strength, fatigue strength and fatigue ratio (the ratio of fatigue strength to tensile strength) of RuT450 with different temperatures are plotted in Fig. 9. It can be seen that with the increase of temperature, both the tensile strength and fatigue strength decrease significantly, but the fatigue ratio increases, which means that the decreasing extent of fatigue strength becomes smaller.

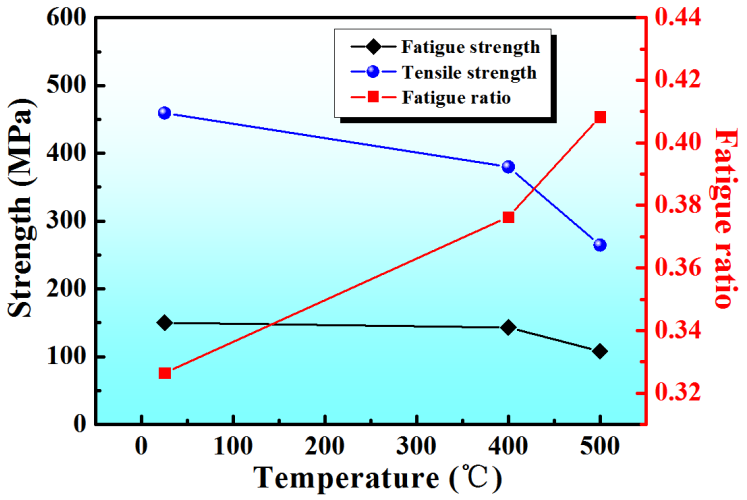


**Figure 9. Variation trends of fatigue strength, tensile strength and fatigue ratio with temperature.**

The RT hardnesses of RuT450 after tensile tests at RT, 400°C and 500°C are shown in Table 2. One can see that the highest hardness is that after tests at 400°C.

**Table 2. The RT harnesses of RuT450 after tests with different temperatures**

| Temperature | RT | 400℃ | 500℃ |
|---|---|---|---|
| HV($N/mm^2$) | 219 | 242 | 223 |

## 4. Discussion

### 4.1 Mechanism of fatigue

Combined with the tensile curve, the hardness variation of RuT450 can be discussed. Dynamic strain aging of RuT450 occurs during the tensile tests at 400°C and 500°C. It means that at high temperature, carbon atoms gain activation energy and diffuse, pinning dislocations, thus hindering the slip of dislocations. This process is accompanied by the precipitation of carbon atoms and a degree of structural transformation. As shown in Fig. 10, after high temperature fatigue test, the microstructure near the fracture surface behaves in a slight change; the area proportion of ferrite, pearlite and graphite has changed, as listed in Table 3 (five fields of view of each specimen were selected and the listed data are average values). It can be seen that the proportion of pearlite decreases slightly with the increase of experimental temperature, but the overall uniformity of the matrix increases, so the hardness increases. In addition, the dispersion of the fatigue data will be slightly reduced due to the improvement of the homogeneity of the structure of the material, as shown in Fig. 4d, however, at RT, the dispersion of data is the largest.

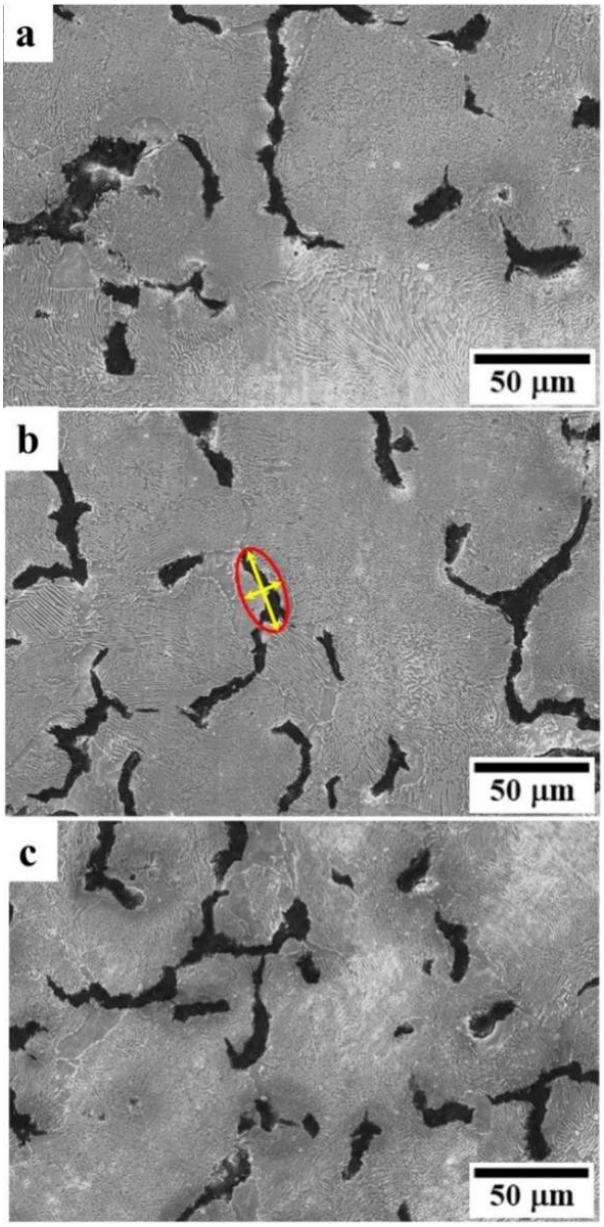


**Figure 10. Microstructure (near the fracture surface) of HCF samples under different temperatures: (a) RT, (b) 400℃, (c) 500℃.**

**Table 3. The area proportion of RuT450 and ratio of graphite at different test temperatures**

| Phase | Pearilite | Ferrite | Graphite | Ratio |
|---|---|---|---|---|
| **RT** | 80.1% | 14.8% | 5.1% | 2.53 |

| | | | | |
|---|---|---|---|---|
| **400℃** | 77.7% | 15.4% | 6.9% | 1.95 |
| **500℃** | 74.9% | 16.2% | 8.8% | 1.99 |

In addition, the changes of graphite morphology after fatigue at different temperatures were also calculated. And the ratio of the major axis to the minor axis (the graphite is regarded as an ellipse, as shown in the red and yellow part of Fig. 10b) decreases with the increase of temperature, corresponding values can be found in Table 3.

The change of the above ratios shows that the graphite of RuT450 tends to be activated under high temperature. This indicates that the vermicular graphite at high temperature is more spherical than that at RT, and the stress concentration at the graphite tip is also lower. Hereafter, the word "graphite blunting" is used for vermicular graphite getting more spherical at high temperature for short. According to Fig. 6, Fig. 7 and Fig. 8 and the previous research results [24-28], it is known that cracks initiated at the interface between graphite and matrix under fatigue load. After initiation, the cracks propagated along the matrix and form the main cracks through the bridging of the secondary cracks.

Graphite blunting reduces the stress concentration and makes the crack initiation more difficult, so it can improve the crack initiation life of cast iron. Pearlite is a harder phase with higher crack propagation threshold, however under high temperature, due to the decrease of pearlite proportion, the hindering effect of matrix on crack propagation decreases, and the crack growth life decreases. The area proportion of propagation zone also decreases, which just confirms the change rule of the propagation area in Fig. 5.

As mentioned above, the fatigue strength and fatigue life of RuT450 are controlled by two factors: graphite blunting increases the difficulty of crack initiation and increases the initiation life; while the microstructure transformation reduces the difficulty of crack propagation and reduces the propagation life. The mechanism

mentioned above is the reason why the fatigue ratio increases with the increase of temperature at 400 °C. The schematic diagram of the above mechanism is shown in Fig. 11.

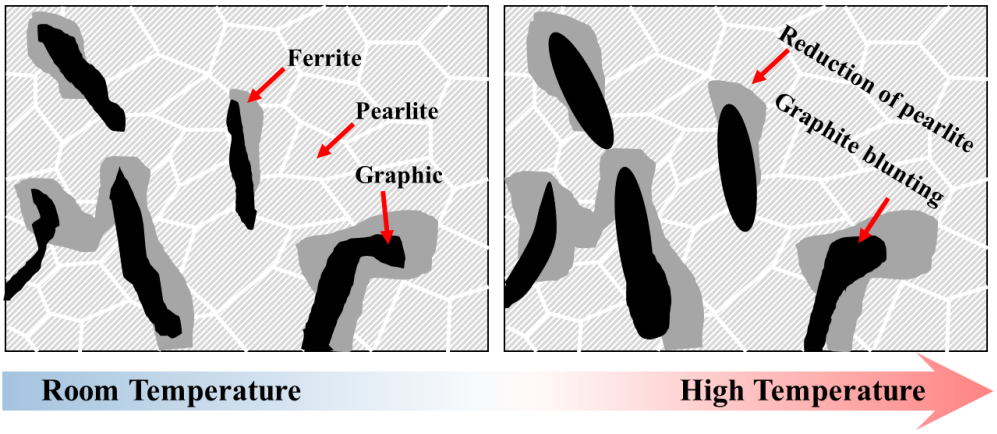


**Figure 11. Schematic diagram of the microstructures of RuT450 under HCF at different temperatures**

In addition, when the temperature is higher than 446°C the mechanical properties of cast iron decrease obviously due to ferrite grain boundary sliding[29-31]. At 500°C, because the temperature is higher than the sliding temperature of ferrite grain boundary, the crack propagation resistance of the material further decreases, and the fatigue strength is greatly reduced by grain boundary oxidation and phase boundary oxidation. This is also the reason why the tensile and fatigue properties become worse at 500°C.

### 4.2 Prediction of fatigue strength

According to the discussion in "4.1 Mechanism of fatigue", the fatigue strength prediction of vermicular graphite cast iron should be based on the microstructure and graphite morphology at different temperatures. Based on the analysis of the conditions of grain boundary blocking slip, Tanaka et al. [32] proposed the fatigue threshold of crack propagation ($K_{th}$):

$$\sigma_{th} = \frac{K_c^m}{\sqrt{\pi(a + w_0)}} + \sigma_{fr}\frac{2}{\pi}\cos^{-1}\left(\frac{a}{a + w_0}\right), \quad (4)$$

$$K_{th} = 2\sigma_{th}\sqrt{\pi a}, \quad (5)$$

Where: $w_0$——width of slip band;

$a$ ——length of crack;

$\sigma_{fr}$——friction stress of dislocation motion;

$K_c^m$——critical value of micro-stress intensity factor.

For vermicular graphite cast iron, its fatigue strength is affected by the proportion of ferrite, pearlite, graphite and graphite morphology. So the fatigue strength ($\sigma_w$) can be expressed as follow:

$$\sigma_w = m\frac{f_1(P)}{f_2(F)f_3(G)f_4(r)}, \quad (6)$$

Where: $P$——area proportion of peralite;

$F$——area proportion of ferrite;

$G$——area proportion of graphite;

$r$——ratio of the major axis to the minor axis of graphite.

And $\boldsymbol{m}$ is a material factor. In Eq. (6), $\boldsymbol{r}$ is positively correlated with the stress concentration factor. Fatigue strength can be regarded as the critical stress of graphite tip crack without propagation, so, its value must be inversely proportional to the stress concentration factor. Therefore, the effect can be expressed as the mean value of the ratio of all graphite major axes ($\boldsymbol{c_i}$) and minor axes ($\boldsymbol{a_i}$):

$$R = f_4(r) = \frac{1}{n}\sum_{i=1}^{n}\frac{c_i}{a_i}. \quad (7)$$

Considering that in the process of HCF, the graphite phase boundary debonding occurs under tensile load (regarded as micro-cracks), some cracks must be located in

the pearlite region, and the other part is in the ferrite region. In this prediction method, its proportion may be considered to be the same as that of the corresponding matrix area proportion. Meanwhile, it is considered that the macro-scale crack growth threshold is the comprehensive reflection of the number of cracks and the threshold value of single-phase. According to Eq. (5), the crack growth threshold is proportional to the critical stress, so:

$$\frac{f_1(P)}{f_2(F)f_3(G)} = q\frac{\Delta K_{th,p}\cdot P_{Area,p}}{\Delta K_{th,f}\cdot P_{Area,f}\cdot \Delta K_{th,g}\cdot P_{Area,g}}. \qquad (8)$$

$$\frac{f_1(P)}{f_2(F)f_3(G)} = q\frac{\Delta K_{th,p}.P_{Area,p}}{\Delta K_{th,f}.P_{Area,f}.\Delta K_{th,g}.P_{Area,g}}$$

And $q$ is a material correction factor. $\Delta K_{th,p}$, $\Delta K_{th,f}$ and $\Delta K_{th,g}$, are crack growth threshold of pearlite, ferrite and graphitic, $P_{Area,p}$, $P_{Area,f}$, $P_{Area,g}$, are corresponding area proportion, respectively. In addition, the sum of the three ($P_{Area,p}$, $P_{Area,f}$, $P_{Area,g}$ ) is 100%. So, Eq. (6) can be transformed into Eq. (9) as follow:

$$\sigma_w = m\frac{f_1(P)}{f_2(F)f_3(G)f_4(r)} = \frac{k}{R}\frac{P_{Area,p}}{(1-P_{Area,p}-P_{Area,g})P_{Area,g}}. \qquad (9)$$

The material factor $k = \dfrac{mq\Delta K_{th,p}}{\Delta K_{th,f}\Delta K_{th,g}}$ (unit is MPa) which reflects the matrix strength and the difficulty of crack propagation can be calculated by fitting the data in Table 3. Another vermicular graphite cast iron, RuT400, was employed to verify the life prediction model above [16]. Whether the parameter $k$ can be obtained by non-fitting method and its physical significance still need to be further studied. The results of fatigue strength prediction are shown in Fig. 12 and Table 4, it can be found that all errors of this prediction method are less than 10%.

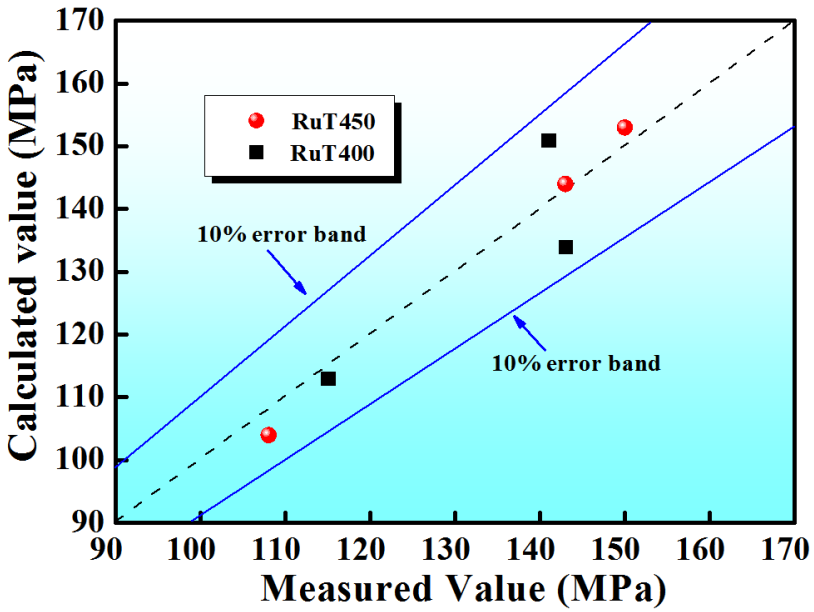


**Figure 12. The calculated vs. experimental values for fatigue strength.**

**Table 4. Results of fatigue strength prediction of RuT450 and RuT400**

| Material | Temperature (℃) | *k* | Measured value (MPa) | Calculated value (MPa) | Error (%) |
|---|---|---|---|---|---|
| RuT450 | RT | 254 | 150 | 153 | 2.0 |
| | 400°C | | 143 | 144 | 0.7 |
| | 500°C | | 108 | 104 | 3.7 |
| RuT400 | 300°C | 1922 | 141 | 151 | 7.1 |
| | 400°C | | 143 | 134 | 6.3 |
| | 500°C | | 115 | 113 | 0.2 |

## 5. Conclusions

The HCF behaviors of vermicular graphite casts RuT450 at different temperatures, fatigue fracture morphologies, failure mechanisms and fatigue strength

prediction were studied in this work. The main conclusions are summarized as follows:

1) The fatigue strength and tensile strength of vermicular graphite cast iron decrease with the increase of temperature, however, the hardness and fatigue ratio at RT (after HCF tests) have no similar changing trends. The tensile and fatigue properties of RuT450 are affected by both dynamic strain aging effect and ferrite grain boundary sliding.

2) The fatigue crack mainly initiated at the interface between graphite and matrix at the edge of the sample, and the main crack was formed by bridging the secondary cracks. At high temperature, the blunting of vermicular graphite tips can increase the fatigue crack initiation life, while the changes of matrix structure will reduce the crack growth life.

3) A fatigue strength prediction method which based on graphite morphology and matrix micro-structure has been proposed. By this way, the temperature influences are transformed into parameters that can be obtained from metallographic observation. This method can predict the HCF strength of vermicular graphite cast iron accurately.

## Conflicts of interest

The authors declare no conflicts of interest.

## Statement of author contribution

M. X. Zhang and Z. F. Zhang conceived of the presented idea. M. X. Zhang wrote the manuscript. J. C. Pang and S. X. Li revised the manuscript. L.J. Meng completed the mechanical properties and microscopic characterization tests. Q. Y. Liu, and A. L. Jiang verified the analytical methods. All authors discussed the results and contributed to the final manuscript.

## Acknowledgments

The authors would like to thank Dr. C. H. Li for her help of SEM observations. This work is supported by the National Nature Science Foundation of China (NSCF) under Grant No. 51871224, the Science Fund of State Key Laboratory of Engine Reliability (SKLER) and LiaoNing Revitalization Talents Program under Grant Nos. XLYC1808027.

## References

[1] Xin Q. Overview of diesel engine applications for engine system design - part 2: general performance characteristics. SAE Tech. Papers 1 (2001).

[2] Dawson S, Schroeder T, Practical applications for compacted graphite iron, AFS Trans. 47 (2004) 1.

[3] Cui X P, Liu H F, Wang C G, et al. Application status and development direction of automotive exhaust manifold materials, Casting, 57 (2008) 1001

[4] Hatton A, Engstler M, Leibenguth P, et al. Characterization of graphite crystal structure and growth mechanisms using FIB and 3D image analysis, Adv. Eng. Mater. 13 (2011) 136.

[5] Meyers M A , Chawla K K, Mechanical behavior of materials, Cambridge University Press, Cambridge, New York, 2008.

[6] Nie L L, Zhang M X, Zhu L B, et al. Fatigue life prediction of motor-generator rotor for pumped-storage plant. Eng. Fail.Anal, 79 (2017) 8.

[7] Jing G X, Zhang M X, Qu S, et al. Investigation into diesel engine cylinder head failure. Eng. Fail.Anal, 90 (2018) 36.

[8] Xu H. Fatigue strength design. China Machine Press, Beijing, 1981.

[9] Diaconu V L, Sjogren T, Skoglund P, et al. Influence of molybdenum alloying on thermomechanical fatigue life of compacted graphite irons. Inter. J. Cast Met. Res, 25 (2012) 277.

[10] Andresem P, Antolovich B, Antolovich S D, et al, ASM Handbook, Volume 19: Fatigue and Fracture, ASM International, United States of America, 1996.

[11] Lyu Y, Sun Y, Liu S, et al. Effect of tin on microstructure and mechanical properties of compacted graphite iron, Int. J. Cast Met. Res. 28 (2015) 263.

[12] Ochi Y, Masaki K, Takashi M F. Effect of shot-peening treatment on high cycle fatigue property of ductile cast iron. Inter. J. Fatigue, 23 (2001) 441.

[13] Sun Z D, Bathias C. High Frequency Fatigue crack propagation behavior of a spheroidal graphite cast iron. SAE Trans, 110 (2001) 714.

[14] Matteis, P, Scavino, G, Castello, A, et al. High-cycle fatigue resistance of si-mo ductile cast iron as affected by temperature and strain rate. Met. Mater. Trans. A, 46 (2015) 4086.

[15] Xu R, Yang Z, Li J P, et al. Effect of creep rate on high cycle fatigue properties of vermicular graphite cast iron. Hot Working Tech, 03 (2020) 35.

[16] Liu Q Y, Zhu G, Pang J C, et al. High-cycle fatigue properties prediction and damage mechanisms of RuT400 compacted graphite iron at different temperatures. Mater. Sci. Eng. A, 764 (2019) 138248.

[17] Meng L J, Zhang M X, Li Y J, et al. Tensile and fatigue properties of vermicular graphite cast iron RuT400 and RuT450. Shanghai Met, 04 (2020) 18.

[18] Tartera J, Llorca N I, Marsal M, et al. Similarities of nucleation and growth of spheroidal and compacted graphite, Int. J. Cast Met. Res. 16 (2003) 131.

[19] Chuang C, Singh D, Kenesei P. et al. 3D quantitative analysis of graphite morphology in high strength cast iron by high-energy X-ray tomography, Scripta Mater. 106 (2015) 5.

[20] Liu Y, Li Y, Xing J, et al. Effect of graphite morphology on the tensile strength and thermal conductivity of cast iron，Mater. Charact. 144 (2018) 155.

[21] Y. L.Lee, J. Pan, R.B. Hathaway, M. E. Barkey, *Fatigue testing and analysis: theory and practice*. Butterworth-Heinemann, Waltham, **2005**.

[22] Nelson S, Ladani L, Topping T, et al. Fatigue and monotonic loading crack nucleation and propagation in bimodal grain size aluminum alloy. Acta Mater, 59 (2011) 3550.

[23] Yao J C. Dynamic strain aging behavior of extruded al-3.5mg-0.2sc alloy under fatigue loading, PhD Dissertations. Technology University of Shenyang, 5 (2016) 17.

[24] Zhang M X, Pang J C, Qiu Y, et al. Thermo-mechanical fatigue property and life prediction of vermicular graphite cast iron. Mater. Sci. Eng. A, 698 (2017) 63.

[25] Zhang M X, Pang J C, Qiu Y, et al. Influence of microstructure on the thermo-mechanical fatigue behavior and life of vermicular graphite cast irons. Mater. Sci. Eng. A, 771 (2019) 138617.

[26] Zou C L, Pang J C, Chen L J, et al. The low-cycle fatigue property, damage mechanism and life prediction of compacted graphite iron: Influence of strain rate. Inter. J. Fatigue, 135 (2020) 105576.

[27] Liu R, Tian Y Z, Zhang Z J, et al. Fatigue strength plateau induced by microstructure inhomogeneity. Mater. Sci. Eng. A, 702 (2017) 259.

[28] Qiu Y, Pang JC, Zhang MX, et al. Influence of experimental temperature on the high-cycle fatigue properties of compacted graphite iron, Int. J. Fatigue. 112 (2018) 84.

[29] Qiu Y, Pang J C, Li S X, et al. Influence of thermal exposure on microstructure evolution and tensile fracture behaviors of compacted graphite iron. Mater. Sci. Eng. A 664 (2016) 75.

[30] Qiu Y, Pang J C, Yang E N et al. Transition of tensile strength and damage mechanisms of compacted graphite iron with temperature. Mater. Sci. Eng. A, 667 (2016) 290.

[31] Zou C L, Pang J C, Zhang M X, et al. The high cycle fatigue, deformation and fracture of compacted graphite iron: Influence of temperature，Mater. Sci. Eng. A 724 (2018) 606.

[32] Tanaka K, Nakai Y, Yamashita M. Fatigue growth threshold of small cracks. Int. J. Fract. 17 (1981) 519.